# Projection and Reconstruction-Based Noise Filtering Methods in Cone Beam CT

Benedikt Lorch[1], Martin Berger[1,2], Joachim Hornegger[1,2], Andreas Maier[1,2]

[1]Pattern Recognition Lab, FAU Erlangen-Nürnberg
[2]Research Training Group 1773 “Heterogeneous Image Systems”
benedikt.lorch@fau.de

**Abstract.** A reduction of the radiation dose in computed tomography typically leads to more noise in the acquired projections. Here filtering methods can help to reduce the noise level and preserve the diagnostic value of the low-dose images. In this work, six variants of Gaussian and bilateral filters are applied in both projection and reconstruction domain. Our comparison of noise reduction and image resolution shows that 2D and 3D bilateral filtering in the projection domain can reduce the noise level, but must be applied carefully to avoid streaking artifacts. By smoothing homogeneous regions while preserving sharp edges, the 3D bilateral filter applied in the reconstruction domain yielded the best results in terms of noise reduction and image sharpness.

## 1 Introduction

In cone beam computed tomography (CBCT), x-rays are used to acquire projection images of patient anatomies. A general goal in CBCT is to reduce the radiation dose while preserving the diagnostic value of the images. However, a low radiation dose typically leads to higher noise level in the reconstructions. In clinical practice reconstruction filter kernels are used that incorporate low-pass filters into the ramp filtering step during image reconstruction. This process is similar to Gaussian filtering, as the filtering operations are by definition linear and are therefore not able to preserve image resolution properly.

Non-linear filtering methods have been proposed that aim to keep sharpness and resolution as constant as possible while decreasing noise in homogeneous areas. In analytic reconstruction, adaptive weighting of the projection data can be used prior to reconstruction to reduce noise [1,2]. A different approach is to apply noise filtering after reconstructing the 3D object, e.g. by bilateral or wavelet-based filtering [3,4]. Less work has been done on non-linear filtering in the projection domain. Manduca et al. proposed to use an adaptive 2D bilateral filter on the projection images [5]. Further, 2D [6] as well as 3D [7] anisotropic filtering was applied in the projection domain, where the latter uses the view angles of a circular CBCT trajectory as a third dimension.

In this work, we also investigate a 3D bilateral filter in the projection domain along with convolution-based and non-linear, edge-preserving noise filtering methods on projections and reconstructions. Through comparison of all methods we identify which domain is best suited for the individual filtering approach.

## 2 Materials and Methods

### 2.1 Filtering Methods

In total, we evaluated six variants of 2D and 3D Gaussian and bilateral filtering. The Gaussian filter is a simple convolution of the input image with a Gaussian function used to reduce image noise and smooth edges. The filtered image function $\hat{f}$ is given by the convolution function

$$\hat{f}(\boldsymbol{x}, \sigma_g) = \sum_{\boldsymbol{\mu} \in \Omega} f(\boldsymbol{\mu}) \cdot c(\boldsymbol{x}, \boldsymbol{\mu}, \sigma_g)$$
$$c(\boldsymbol{x}, \boldsymbol{\mu}, \sigma_g) = \frac{1}{\sqrt{(2\pi\sigma_g)^d}} \exp\left(-\frac{1}{2\sigma_g^2}\,(\boldsymbol{x} - \boldsymbol{\mu})^{\mathrm{T}}(\boldsymbol{x} - \boldsymbol{\mu})\right) \quad , \tag{1}$$

where $\boldsymbol{x}$ is the geometric position in the image, $\Omega$ is the set that defines the neighborhood of $\boldsymbol{x}$ and $\sigma_g$ is the spherical standard deviation of the $d$-dimensional Gaussian filter kernel. An advantage of Gaussian filters is that they can be applied by a fast convolution, however they are also known to blur edge information.

We also used the non-linear bilateral filter [3], which combines the smoothing of a Gaussian with an edge-preserving component by adjusting the filter kernel based on the local intensities of the image. The filtered image $\widetilde{f}$ is computed by

$$\widetilde{f}(\boldsymbol{x}, \sigma_g, \sigma_p) = \frac{1}{k(\boldsymbol{x}, \sigma_p)} \sum_{\boldsymbol{\mu} \in \Omega} f(\boldsymbol{x}) \cdot c(\boldsymbol{x}, \boldsymbol{\mu}, \sigma_g) \cdot s(f(\boldsymbol{x}), f(\boldsymbol{\mu}), \sigma_p)$$
$$s(f(\boldsymbol{x}), f(\boldsymbol{\mu}), \sigma_p) = \exp\left(-\frac{1}{2\sigma_p^2}(f(\boldsymbol{x}) - f(\boldsymbol{\mu}))^2\right) \quad , \tag{2}$$

where $\sigma_p$ is the standard deviation used for the photometric distance. The kernel function is now given by $c(\boldsymbol{x}, \boldsymbol{\mu}, \sigma_g) \cdot s(f(\boldsymbol{x}), f(\boldsymbol{\mu}), \sigma_p)$, hence the normalization factor $k(\boldsymbol{x}, \sigma_p)$ is formed by the sum of all kernel values. If the intensity difference between $f(\boldsymbol{x})$ and $f(\boldsymbol{\mu})$ becomes high, e.g. due to an edge, the weight for $f(\boldsymbol{\mu})$ becomes low which prevents edges from being smoothed out.

In the projection domain, Gaussian (GP-2D) and bilateral filtering (BP-2D) were applied to all 2D projection images. To further reduce noise we also applied 3D Gaussian (GP-3D) and bilateral filtering (BP-3D) on the complete stack of projections. Note that in this case the third dimension refers to the view angle, as we aim to incorporate information from neighboring projections. Finally, these measurements were compared to 3D Gaussian (GV-3D) and 3D bilateral filtering (BV-3D) applied as pure post-processing on the volume which was reconstructed from the noisy projections.

### 2.2 Data and Setup

To obtain the same projection data with different noise levels, we simulated an CBCT scan using the Forbild head phantom[1]. The focal length was set to

[1] http://www.imp.uni-erlangen.de/forbild

1200mm and the phantom was centered at the rotation center at a distance of 600mm to the x-ray source. The detector size was set to 640x480 pixels with an isotropic pixel size of 1.2mm. We simulated a circular trajectory around the z-axis, acquiring a short-scan with 248 projections and an angular increment of 0.869°. For noise simulation a monochromatic absorption model was used, releasing 50 000 photons with an energy of 80keV for simulating a moderate noise level and 30 000 photons with an energy of 50keV for an increased noise level. As ground truth we also generated a 3D volume of the Forbild phantom with a resolution of 1024x1024x1024 voxels and an isotropic voxel size of 0.25mm.

The FDK method was used for reconstruction [8]. We applied a Ram-Lak filter without window function to ensure that the resolution is not influenced by the ramp-filtering step. Noise filtering on the projections was conducted at the beginning, filtering on the reconstruction was done at the end of the pipeline.

To quantify the noise level, we calculated the standard deviation $\sigma_{sd}$ inside a box shaped homogeneous region with a side length of 16mm. The central section of the box is depicted in Fig. 1. For measuring the residual resolution of the filtered images, we computed the modulation transfer function (MTF). Therefore, the mean of 150 line profiles was taken along the inner edge of the scull bone as shown in Fig. 1 to minimize the influence of streak and noise artifacts. Then the MTF is calculated by the Fourier transform of the derivative of the mean line profile. The achieved resolution was determined by the frequency that corresponds to a ten percent residual of the magnitude spectrum's maximum. In order to evaluate the filtering methods' performance w.r.t. their parameters, we used a grid search approach where the upper and lower bounds of the parameter range have been adjusted heuristically.

## 3 Results

In Fig. 1 and Fig. 2, the reconstructions are shown for the 80keV and the 50keV datasets, respectively. The residual noise $\sigma_{sd}$ was fixed as denoted in Table 1. In both datasets, the BV-3D produces the best results with the highest resolution. The BP-2D gives the sharpest results of the projection domain approaches, closely followed by BP-3D. All Gaussian methods show a reduced sharpness compared to bilateral filtering. However, the BP-3D and the BP-2D reveal increased streaking artifacts especially in the 50keV dataset. Fig. 3 and Fig. 4 compare the achieved MTF values w.r.t. the measured noise level $\sigma_{sd}$. A high $\sigma_p$ degenerates the bilateral filter to a Gaussian filter as depicted in Fig. 3a. In Fig. 3b, we can

**Table 1.** Resolution measured at 10% MTF for a fixed noise level $\sigma_{sd}$. Given an isotropic voxel size of 0.25mm, the theoretical maximum is given by 10 lp/cm.

| 10% MTF in lp/cm | GP-2D | GP-3D | BP-2D | BP-3D | GV-3D | BV-3D |
|---|---|---|---|---|---|---|
| 80keV dataset ($\sigma_{sd} = 0.01$) | 4.81 | 4.96 | 5.88 | 5.60 | 4.46 | 6.79 |
| 50keV dataset ($\sigma_{sd} = 0.07$) | 5.01 | 5.08 | 6.11 | 5.95 | 4.81 | 7.34 |

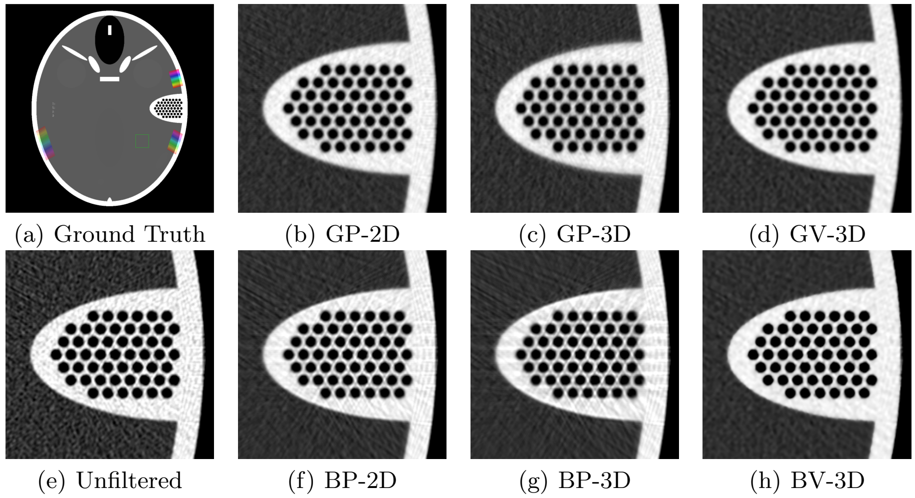


**Fig. 1.** Filtering methods with $\sigma_{sd} = 0.01$ on the 80keV dataset. The box in (a) depicts a section of the homogeneous region where $\sigma_{sd}$ was calculated. The colored lines indicate the line profiles used for the MTF. Visualization window set to $[0.10, 0.52]$ cm$^2$/g.

see that the Gaussian methods perform similarly well, yet, the projection based methods show a slightly higher MTF value. Fig. 4 displays the MTF results for bilateral filtering methods.

By decreasing $\sigma_p$, results yield a higher resolution until a turning point, at which resolution as well as noise reduction do not vary anymore. Quantitative MTF measurements support the visual impressions and are given in Table 1.

## 4 Discussion

In this work, we compared Gaussian and bilateral filtering methods in projection and reconstruction domain. From Fig. 3b we can see that the projection-based Gaussian methods slightly exceed the GV-3D methods in terms of resolution, which can be due to the high-pass effect of the subsequent ramp filtering step. Nevertheless, BP-2D and BP-3D appear sharper than GP-2D and GP-3D. However, BP-3D reveals streak artifacts especially at sharp structures (cf. Fig. 1 and Fig. 2), which might be caused by incorporating non-correct information of the neighboring projections. BP-2D is also affected by less dominant streak artifacts, whereas BV-3D showed good noise suppression while preserving sharp edges.

In the 50keV dataset all images reveal streaking artifacts caused by the high amount of noise. In case of BP-2D and BP-3D the smooth areas in homogeneous regions without streaks indicate that the photometric kernel was not wide enough to capture high-noise peaks in the projection domain. While all projection-based filters yield blurred edges, 3D filtering on the reconstructions preserves structure well but also shows slightly increased streaking compared to the GV-3D method.

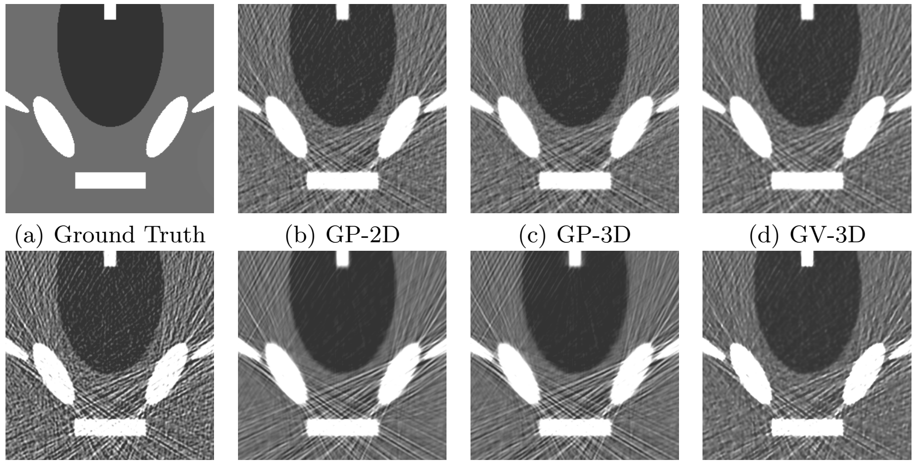

(a) Ground Truth (b) GP-2D (c) GP-3D (d) GV-3D

(e) Unfiltered (f) BP-2D (g) BP-3D (h) BV-3D

**Fig. 2.** Filtering methods with $\sigma_{sd} = 0.07$ on the 50keV dataset. Visualization window set to $[0.20, 0.80]$ $\mathrm{cm}^2/\mathrm{g}$.

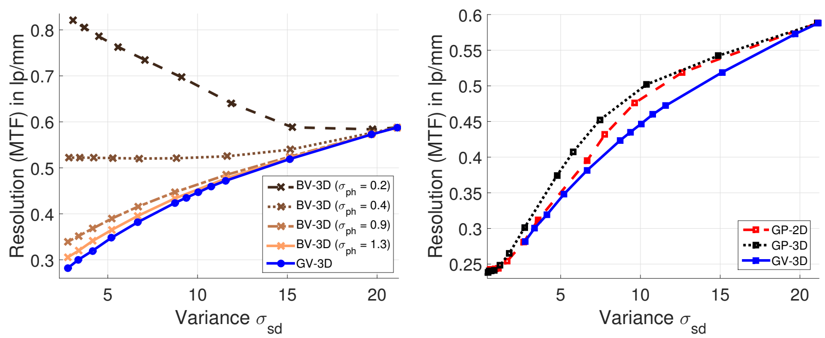


(a) Gaussian vs. bilateral filtering (b) Comparison of Gaussian filters

**Fig. 3.** Comparison of resolution and noise level of Gaussian and bilateral filtering on the 80keV dataset.

Fig. 4 compares several variants of bilateral filtering with different photometric distances. Some methods achieve a greater MTF than the unfiltered image which seems incorrect. This can be explained as we use a measure that is only suited for linear methods on non-linear methods.

We have seen that bilateral filtering in the reconstruction domain gives promising results. Also projection-based filtering has shown its ability to preserve edges, however these methods should be applied carefully to avoid irregular streaking artifacts. For future work, we plan to combine 2D and 3D noise filtering in projection and reconstruction domain. Further, we plan to confirm our results by using a model-observer evaluation pipeline.

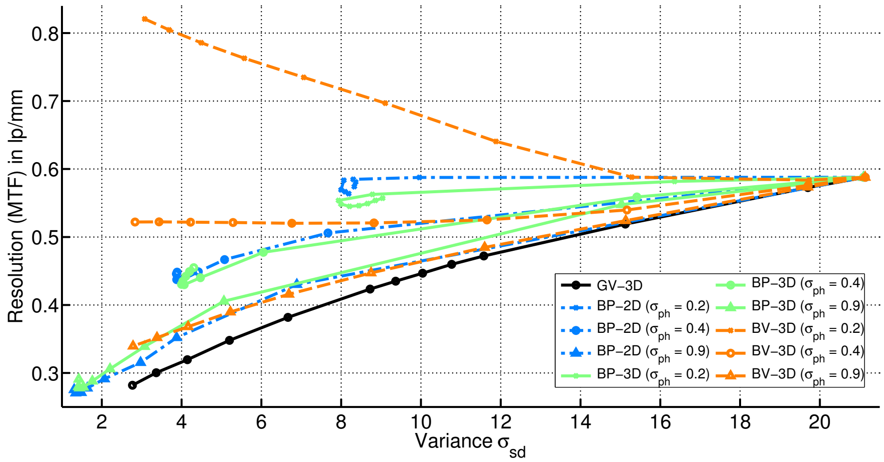


**Fig. 4.** Bilateral filtering with different $\sigma_p$ on projections and reconstructions.

**Acknowledgements**

The authors gratefully acknowledge funding of the Research Training Group 1773 "Heterogeneous Image Systems" and the Erlangen Graduate School in Advanced Optical Technologies (SAOT) by the German Research Foundation (DFG).

## References

1. Kachelrieß M, Watzke O, Kalender WA. Generalized multi-dimensional adaptive filtering for conventional and spiral single-slice, multi-slice, and cone-beam CT. Medical Physics. 2001;28(4):475–490.
2. Zeng GL. Noise-weighted spatial domain FBP algorithm. Medical Physics. 2014;41(5):051906.
3. Tomasi C, Manduchi R. Bilateral filtering for gray and color images. In: Computer Vision, 1998. Sixth International Conference on; 1998. p. 839–846.
4. Borsdorf A, Raupach R, Flohr T, Hornegger J. Wavelet based Noise Reduction in CT-Images Using Correlation Analysis. IEEE Transactions on Medical Imaging. 2008;27(12):1685–1703.
5. Manduca A, Yu L, Trzasko JD, Khaylova N, Kofler JM, McCollough CM, et al. Projection space denoising with bilateral filtering and CT noise modeling for dose reduction in CT. Medical physics. 2009;36(11):4911–4919.
6. Dirk Schäfer MG Peter van de Haar. Comparison of Gaussian and non-isotropic adaptive projection filtering for rotational 3D X-ray angiography. In: Leahy RM, Qi J, editors. Fully Three-Dimensional Image Reconstruction in Radiology and Nuclear Medicine; 2013. p. 130–133.
7. Maier A, Wigström L, Hofmann H, Hornegger J, Zhu L, Strobel N, et al. Three-dimensional anisotropic adaptive filtering of projection data for noise reduction in cone beam CT. Medical Physics. 2011;38(11):5896–5909.
8. Feldkamp L, Davis L, Kress J. Practical cone-beam algorithm. JOSA A. 1984;1(6):612–619.